Available online at www.sciencedirect.com
ScienceDirect
Astroparticle Physics 26 (2007) 367–377
Astroparticle Physics
www.elsevier.com/locate/astropart

Limits on the transient ultra-high energy neutrino flux from gamma-ray bursts (GRB) derived from RICE data

D. Besson [a], S. Razzaque [b,*], J. Adams [c], P. Harris [c]

[a] Department of Physics and Astronomy, University of Kansas, Lawrence, KS 66045, United States
[b] Department of Astronomy and Astrophysics and Department of Physics, Pennsylvania State University, University Park, PA 16802, United States
[c] Department of Physics, University of Canterbury, Christchurch, New Zealand

Received 5 June 2006; received in revised form 20 July 2006; accepted 21 July 2006
Available online 1 September 2006

Abstract

We present limits on ultra-high energy (UHE; $E_\nu > 10^{15}$ eV) neutrino fluxes from gamma-ray bursts (GRBs), based on recently presented data, limits, and simulations from the RICE experiment. We use data from five recorded transients with sufficient photon spectral shape and redshift information to derive an expected neutrino flux, assuming that the observed photons are linked to neutrino production through pion decay via the well-known "Waxman–Bahcall" prescription. Knowing the declination of the observed burst, as well as the RICE sensitivity as a function of polar angle and the previously published non-observation of any neutrino events allows an estimate of the sensitivity to a given neutrino flux. Although several orders of magnitude weaker than the expected fluxes, our GRB neutrino flux limits are nevertheless the first in the PeV–EeV energy regime. For completeness, we also provide a listing of other bursts, recorded at times when the RICE experiment was active, but requiring some assumptions regarding luminosity and redshift to permit estimates of the neutrino flux.

Keywords: Neutrinos; GRBs; Neutrino telescope; Neutrino astronomy; Single source predictions; RICE

1. Introduction

1.1. Gamma-ray bursts

Gamma-ray bursts (GRBs) are the most energetic explosions in the Universe, releasing upwards of $\sim 10^{51}$ ergs of radiation energy in γ-rays ($\sim$0.1–1 MeV) within a few seconds (see Refs. [1,2] for reviews on GRB observations). The Burst and Transient Source Experiment (BATSE) on board the *Compton Gamma-Ray Observatory* (CGRO) satellite detected bursts at the rate of about 300 per year, in the period 1991–2001, isotropically distributed over the sky. The observed duration of the bursts falls into two categories, long bursts lasting for tens of seconds and short bursts lasting for less than 2 s. The *Beppo*SAX, *High Energy Transient Explorer* (HETE-2) and *SWIFT* satellites are observing GRBs currently on a routine basis. However, the redshift measurement, and hence the total energy estimate, is possible only for a small fraction of the bursts as it requires identification of the GRB host galaxies in optical wave bands.

The unsurpassed γ-ray luminosity naturally make GRBs candidate sources of the observed ultra-high energy cosmic-rays [3,4], many with $\gtrsim 10^{18}$ eV. High energy ($E_\nu \gtrsim 100$ GeV) neutrinos may then be created from the cosmic-rays, as in beam-dump experiments, while propagating in the cosmic photon backgrounds [5–7] and/or at the particle acceleration sites of the sources [8–10]. While diffuse flux estimates are a useful method for calculating the total neutrino energy injection into the universe by GRBs, individual source detection is crucial for understanding the source production processes, and

* Corresponding author.
E-mail address: soeb@astro.psu.edu (S. Razzaque).

0927-6505/$ - see front matter © 2006 Elsevier B.V. All rights reserved.
doi:10.1016/j.astropartphys.2006.07.008

in particular, for verifying whether point sources are the sources of UHE cosmic-rays. For transient sources such as GRBs, individual luminous and bright bursts may dominate the observed diffuse emission as well. A number of authors have calculated expected neutrino production from individual long bursts (short bursts are typically lower in energy output and hence less likely to be detected individually in neutrino telescopes [11–16]). When folded in with a given experimental acceptance, such flux predictions can then be translated into expected sensitivities or, in the case of no detection, upper limits.

1.2. Radiowave neutrino detection

The RICE experiment has goals similar to the larger AMANDA and ICECUBE experiments – both seek to measure UHE neutrinos by detection of Cherenkov radiation produced by neutrino–nucleon interactions. Whereas AMANDA/ICECUBE is optimized for detection of penetrating muons resulting from $\nu_\mu + N \to \mu + N'$, RICE is designed to detect compact electromagnetic and hadronic cascades initiated by charged or neutral current neutrino interactions in a dense medium: $\nu_l(/\bar{\nu}_l) + N \to l^{\pm} + N'$ or $\nu_l(/\bar{\nu}_l) + N \to \nu_l(/\bar{\nu}_l) + N'$ respectively, with $l = e, \mu, \tau$. As the cascade evolves, a charge excess develops as atomic electrons in the target medium are swept into the forward-moving shower via Compton scattering and positrons are depleted via annihilation, resulting in a net charge on the shower front of $Q_{tot} \sim E_s e/4$; E_s is the shower energy in GeV [17–24]. Such cascades produce broadband Cherenkov radiation – for $\lambda_{\text{E-field}}^{\text{Cherenkov}} \gg r_{\text{Moliere}}$, the emitting region approximates a point charge of magnitude Q_{tot} and therefore emits fully coherently; fortuitously, the field attenuation length at such wavelengths in cold polar ice ($\sim$1 GHz) exceeds 1 km [25]. The quadratic rise of the Cherenkov power with neutrino energy, combined with the long attenuation length lead to the expectation that the effective volume of radio-based detectors begin to exceed those of photomultiplier-tube based detectors at a cross-over energy of $\sim$1 PeV [26], leading to neutrino detector arrays consisting of tens of buried radio antennas. The RICE radio antenna detection concept of the Cherenkov radiation produced by an in-ice weak current event is depicted in Fig. 1.

In this paper, we determine model-dependent RICE neutrino flux upper limits for five GRBs, namely 020813, 020124, 050603, 050730 and 050908 for which we have extensive observational data including redshifts. Using calculations published elsewhere of the expected radio-frequency signal strength due to an electromagnetic shower [18,19], the RICE hardware, reconstruction software and simulation [27–29], and a neutrino analysis based on data taken 1999–2005 [29], we can translate an expected neutrino flux from the bursts recorded while RICE was active into an expectation for the RICE neutrino yield. These expectations are valid in an energy regime somewhat higher than those typical of, e.g., previous AMANDA gamma-ray burst studies [12]. Our calculation of expected neutrino fluxes from these GRBs is the most novel aspect of this analysis, and is presented in greater detail herein.

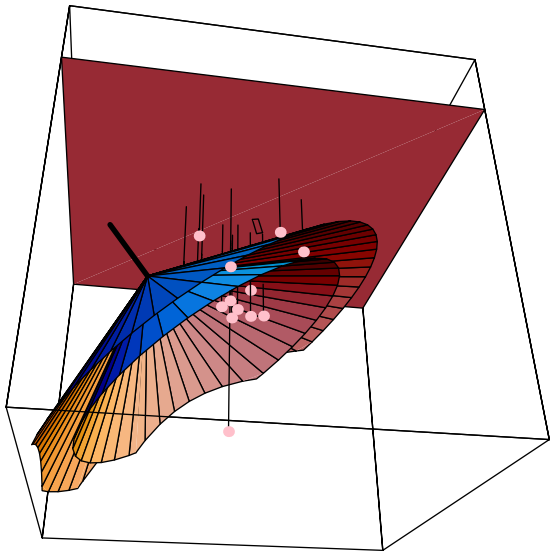

Fig. 1. RICE concept. Shown is an incident neutrino interacting $\sim$100 m below the surface and illuminating the RICE radio antenna array, indicated by spheres and drawn to scale. Horizontal extent is approximately 400 m.

2. Hardware

The RICE experiment presently consists of a 20-channel array of dipole radio receivers, scattered within a 200 m × 200 m × 200 m cube, at 100–300 m depths. The signal from each antenna is boosted by a 36-dB in-ice amplifier, then carried by coaxial cable to the surface observatory, where the signal is filtered (suppressing noise below 200 MHz), re-amplified (either 52- or 60-dB gain), and split – one copy is fed into a CAMAC crate to form the event trigger; the other signal copy is routed into one channel of an HP54542 digital oscilloscope. Four antennas which register "hits" within a 1.25 μs window define an event trigger. "Hits" are defined as a voltage excursion greater in magnitude than a discriminator threshold, determined at the beginning of each run as that threshold which gives approximately 90% livetime. Deadtime is incurred by a full event trigger readout (approximately 10 s of deadtime), the fast software rejection of anthropogenic noise (approximately 10 ms of deadtime per calculation), or the fast hardware rejection of anthropogenic noise (1.2 μs per event). Short-duration pulses broadcast from under-ice transmitters provide the primary calibration signals and are used to verify vertex reconstruction techniques.

Given the known experimental circuit gains and losses [27], the effective volume V_{eff} is calculated as a function of incident E_ν, as an exposure average of the detector con-

figurations. The most important variable is the global discriminator threshold, which is adjusted to maintain an acceptable trigger rate under conditions of varying environmental noise.

Additional details on the RICE shower search procedures are presented elsewhere [29]. The most recent search has resulted in zero neutrino candidates, yielding competitive limits on the incident ultra-high energy neutrino flux at energies above 10^{17} eV.

3. GRB model and neutrino flux calculation

In the most widely accepted GRB model, known as the *fireball-shock model*, the prompt γ-rays are produced by collisions of plasma material moving relativistically (with a bulk Lorentz factor $\Gamma \gtrsim 100$) along a jet (*internal shocks*), i.e., a *fireball*. Late time collisions of jetted material with an external medium (*external shocks*) produce X-ray, UV and optical radiation, collectively known as GRB afterglow (see Ref. [30,31] for reviews). A significant number of nucleons are expected to be present in the jet along with leptons (electrons and positrons). The probable mechanism(s) responsible for the observed photons is/are synchrotron radiation or/and inverse Compton scattering by high energy electrons. These electrons are stochastically accelerated by relativistic shocks via the well-known Fermi mechanism in the tangled local magnetic field resulting in a power-law energy distribution.

Protons are expected to co-accelerate with electrons in the shocks. High energy non-thermal neutrinos are expected to be produced by photonuclear (pγ) interactions of protons with observed prompt γ-rays [8,9] and afterglow photons [10] in these optically thin (for Thomson scattering) environments. In this analysis, we put limits on the Waxman–Bahcall GRB neutrino burst and neutrino afterglow flux models, which are based on the standard fireball-shock model of GRBs. We do not consider in the present work other neutrino flux models, e.g., (i) precursors from GRB jets buried under the stellar surface [32,33]; (ii) GRB *blast-wave* models [34] in which both prompt and afterglow emission arise from the external shocks; (iii) afterglow from GRBs in dense stellar winds [35]; (iv) the *supranova* model [36–38] in which a supernova type remnant shell from the progenitor star is ejected prior to the GRB event (These models are either seldom used to interpret data or there is a lack of evidence, especially from electromagnetic observations, supporting them.) Precursor neutrinos [32,33] below the RICE threshold ($E_\nu \gtrsim 10$ PeV) may be detected by neutrino telescopes (e.g., IceCube) without any detectable electromagnetic counter-part from their optically thick environment.

Below, we detail the prescription we have employed in estimating the expected neutrino fluxes from a GRB with a well-measured γ-ray flux, following closely the calculations of Waxman and Bahcall ([8–10], see also [39,40]).

3.1. GRB observed and model parameters

The isotropic-equivalent γ-ray bolometric energy and luminosity of a GRB at redshift z, given the measured bolometric γ-ray fluence S_γ (typically measured over one decade in energy range) and duration t_{90}, may be calculated as

Energía total del GRB — Energía por unidad de tiempo (Luminosidad)

$$E_{\gamma,\mathrm{iso}} = 4\pi d_{\mathrm{L}}^2 S_\gamma/(1+z); \quad L_{\gamma,\mathrm{iso}} = 4\pi d_{\mathrm{L}}^2 S_\gamma/t_{90}, \tag{1}$$

where d_{L} is the luminosity distance. The actual jetted energy is $(4\pi/\Omega)E_{\gamma,\mathrm{iso}}$, where Ω is the jet opening solid angle (typically ~0.1 rad). The γ-ray energy, arising from shock-accelerated electron synchrotron radiation and/or inverse Compton scattering, is assumed to be a fraction $\varepsilon_{\mathrm{e}} < 1$ of the isotropic-equivalent kinetic energy, $E_{\mathrm{kin,iso}}$, of the relativistic plasma material in the standard fireball-shock model. The shock magnetic field shares another fraction $\varepsilon_{\mathrm{B}} < 1$ of $E_{\mathrm{kin,iso}}$.

The luminosity distances may be calculated using the conversion calculator provided by the NASA Extra galactic Database (NED [41]) for a ΛCDM flat cosmology with $H_0 = 70\ \mathrm{km\ s^{-1}\ Mpc^{-1}}$, $\Omega_{\mathrm{m}} = 0.3$ and $\Omega_\Lambda = 0.7$ ($1\ \mathrm{Gpc} = 3.1 \times 10^{27}$ cm). We have tabulated different observed quantities in Table 1 from 5 GRBs. The calculated values of $E_{\gamma,\mathrm{iso}}$ and $L_{\gamma,\mathrm{iso}}$ are also tabulated for later use. The average fractional RICE livetime over the duration of the burst is also indicated in the last column.

The observed γ-ray spectrum from a GRB may be approximately fitted with a broken power-law (Band fit [42]) as

$$\frac{\mathrm{d}N_\gamma}{\mathrm{d}\epsilon_\gamma} \propto \begin{cases} \epsilon_\gamma^{-\alpha}; & \epsilon_\gamma < \epsilon_{\gamma,\mathrm{b}}, \\ \epsilon_\gamma^{-\beta}; & \epsilon_\gamma > \epsilon_{\gamma,\mathrm{b}}. \end{cases} \tag{2}$$

The spectral indices and break energy $\epsilon_{\gamma,\mathrm{b}}$ from observations (where available) are listed in Table 1. Values with asterisks have been estimated using the phenomenological Ghirlanda relationship [43] as

$$\epsilon_{\gamma,\mathrm{b}} = \frac{300}{1+z}\left(\frac{E_{\gamma,\mathrm{iso}}}{10^{53}\ \mathrm{ergs}}\right)^{0.56}\ \mathrm{keV}. \tag{3}$$

Note, however, that the precise value of $\epsilon_{\gamma,\mathrm{b}}$ is not necessary to estimate the expected neutrino flux in the energy range of our interest, as we calculate in the next subsection.

3.2. Burst neutrinos

reacciones de fotoproduccion

The condition for resonant pγ interaction at Δ^+ energy is $\epsilon'_{\mathrm{p}}\epsilon'_\gamma \simeq 0.3\ \mathrm{GeV}^2$ in the local rest frame of the plasma (We denote primed (unprimed) variables in the plasma rest (lab) frame. The observed variables are redshift-corrected lab variables). On average, the proton loses a fraction $\langle x_{\mathrm{p}\to\Delta^+}\rangle \simeq 0.2$ of its energy in this interaction. The secondary Δ^+, produced by a pγ interaction decays as either $\Delta^+ \to \mathrm{n}\pi^+$ or $\Delta^+ \to p\pi^0$ [53]. The pions further decay as $\pi^+ \to \mu^+\nu_\mu \to \mathrm{e}^+\nu_{\mathrm{e}}\bar{\nu}_\mu\nu_\mu$ or $\pi^0 \to \gamma\gamma$. In what follows, we assume equipartition of energy among the four final state

Positrones y electrones acelerados por el mecanismo de fermi, producen fotones al interaccionar mediante efecto compton inverso o bien radiación sincrotrón

Table 1
Observed and estimated GRB parameters

Energía de cambio de pendiente

GRB	S_γ (ergs/cm^2)	t_{90} (s)	z	d_L (Gpc)	$\epsilon_{\gamma,b}$ (keV)	α	β	$E_{\gamma,iso}$ (ergs)	$L_{\gamma,iso}$ (ergs/s)	RICE $\langle Live\ T\rangle$
050908	5.1×10^{-7}	20	3.35	29.02	21*	–	1.93	1.2×10^{52}	2.6×10^{51}	0.93
050730	4.4×10^{-6}	155	3.97	35.52	71*	–	–	1.3×10^{53}	4.3×10^{51}	0.75
050603	3.4×10^{-5}	10	2.82	23.59	289	0.79	2.15	5.9×10^{53}	2.3×10^{53}	0.92
020124A	6.1×10^{-6}	46	3.20	27.47	87	–	–	1.3×10^{53}	1.2×10^{52}	0.83
020813A	8.4×10^{-5}	89	1.25	8.71	142	–	2.15	3.4×10^{53}	8.6×10^{51}	0.98

leptons from π^+-decay. The observed neutrino break energy corresponding to the Δ^+ resonance is then

$$\epsilon_{\nu,b1} = \frac{0.015\Gamma_i^2}{(1+z)^2}\left(\frac{\epsilon_{\gamma,b}}{\mathrm{GeV}}\right)^{-1}\mathrm{GeV}, \quad (4)$$

where $\epsilon_{\gamma,b}$ is the break energy in the γ-ray spectrum (or the peak energy in the $\epsilon_\gamma^2(dN_\gamma/d\epsilon_\gamma)$ energy spectrum). The synchrotron break energy (above which pions lose significant energy by synchrotron radiation before decaying to neutrinos) in the neutrino spectrum is

$$\epsilon_{\nu,sb} = \frac{10^{11}\Gamma_i}{4(1+z)}\left(\frac{B_i'}{G}\right)^{-1}\mathrm{GeV}, \quad (5)$$

where the magnetic field in the GRB fireball is given by

$$B_i' = \sqrt{\frac{2\varepsilon_B L_{\gamma,iso}}{\varepsilon_e r_i^2 \Gamma_i^2 c}} = 5\times10^4\left(\frac{L_{\gamma,iso}}{10^{52}\ \mathrm{ergs/s}}\right)^{1/2}\left(\frac{\Gamma_i}{300}\right)^{-3}\left(\frac{t_v}{0.01\mathrm{s}}\right)^{-1} G. \quad (6)$$

The typically unknown parameters are $\varepsilon_e \approx \varepsilon_B \approx 0.1$; the Lorentz factor of the GRB fireball is $\Gamma_i \approx 300$ from various fits. The radius of the fireball is $r_i \simeq 2\Gamma_i^2 c t_v$, which varies over a large range depending on Γ_i and the variability time scale (typically, $0.001\ \mathrm{s} \leqslant t_v \leqslant 1\ \mathrm{s}$).

To calculate the expected neutrino flux from the GRB fireball, we assume a shock-accelerated proton luminosity in the fireball $L_{p,iso} \simeq L_{\gamma,iso}$ with energy distributed as a power-law: $dN_p/d\epsilon_p \propto \epsilon_p^{-2}$ up to the maximum energy $\lesssim 10^{20}$ eV. The total proton energy, equal per decade in energy, is then $\sim 10E_{\gamma,iso}$ the γ-ray energy; roughly consistent with the assumed equipartition fraction $\varepsilon_e \sim 0.1$ of $E_{kin,iso}$. Due to interactions of these protons with the observed γ-rays the corresponding neutrino energy flux from the GRB prompt phase, following Eqs. (2), (4) and (5), is given by

$$\epsilon_\nu^2\Phi_\nu^s = \frac{1}{2}\frac{f_\pi}{4}\frac{S_\gamma}{t_{90}}\times\begin{cases}(\epsilon_\nu/\epsilon_{\nu,b1})^{\beta-1}; & \epsilon_\nu < \epsilon_{\nu,b1},\\ (\epsilon_\nu/\epsilon_{\nu,b1})^{\alpha-1}; & \epsilon_{\nu,sb} \geqslant \epsilon_\nu \geqslant \epsilon_{\nu,b1},\\ (\epsilon_{\nu,sb}/\epsilon_{\nu,b1})^{\alpha-1}(\epsilon_\nu/\epsilon_{\nu,sb})^{-2}; & \epsilon_\nu > \epsilon_{\nu,sb},\end{cases} \quad (7)$$

for each neutrino flavor ν_μ, $\bar\nu_\mu$ and ν_e at the source. The factors 1/2 and 1/4 arise due to the WB assumption of equal decay probabilities: $\Delta^+ \to \pi^+/\pi^0$ and energy equipartition among the π^+ decay products, respectively. Here f_π is the conversion efficiency of shock-accelerated protons to pions at the Δ^+ resonance in the GRB fireball. For optically thin sources, such as GRBs, $f_\pi \leqslant 0.2$. The detailed calculation of f_π, which involves many unknown variables, is not relevant here. Moreover, the internal shocks (and thus γ-ray emission) occur over a wide range of r_i which in turn affect f_π. We assume a fixed value $f_\pi = 0.2$ for our calculation which corresponds to a $p\gamma \to \Delta^+$ optical depth of the order of unity. The prefactor in the expression for flux (Eq. (7)) can be written as

$$\mathscr{A} \equiv \frac{f_\pi}{8}\frac{S_\gamma}{t_{90}} = 1.56\times10^{-6}\left(\frac{f_\pi}{0.2}\right)\left(\frac{S_\gamma}{10^{-6}\ \mathrm{ergs/cm^2}}\right)\left(\frac{t_{90}}{10\,\mathrm{s}}\right)^{-1}\mathrm{GeV\,cm^2\,s^{-1}} \quad (8)$$

and the γ-ray spectral indices are $\alpha = 1$, $\beta = 2$ to good approximation (1 erg = 624 GeV). After oscillations in vacuum, the neutrino fluxes for different flavors are $\Phi_{\nu_e+\bar\nu_e} = \Phi_{\nu_\mu+\bar\nu_\mu} = \Phi_{\nu_\tau+\bar\nu_\tau} = \Phi_\nu^s$, each with a duration of $t_{burst} = t_{90}$. We have listed values for these parameters in Table 2 for five bursts.

3.3. Afterglow neutrinos

The GRB afterglow, arising from external forward and reverse shocks, takes place at a radius $r_e = (3E_{kin,iso}/[4\pi n_{ex} m_p c^2 \Gamma_i^2])^{1/3}$, which is much larger than r_i. Here we assume the total jet kinetic energy $E_{kin,iso} = E_{\gamma,iso}/\varepsilon_e \simeq 10E_{\gamma,iso}$ throughout our calculation and $n_{ex} = 1$ atom cm^{-3} is a typical interstellar medium (ISM, dominantly neutral hydrogen) density. The bulk Lorentz factor of the reverse-shocked plasma shell at the time $t = t_{90}$ when the reverse shock has crossed the shell is

Table 2
Burst neutrino flux parameters

GRB	$\mathscr{A}$ (GeV cm^{-2} s^{-1})	$\epsilon_{\nu,sb}$ (GeV)	$\epsilon_{\nu,b1}$ (GeV)	t_{burst} (s)
050908	4.0×10^{-7}	9.5×10^7	3.4×10^6	20
050730	4.4×10^{-7}	6.4×10^7	7.7×10^5	155
050603	5.3×10^{-5}	1.2×10^7	3.2×10^5	10
020124A	2.1×10^{-6}	4.6×10^7	8.8×10^5	46
020813A	1.5×10^{-5}	1.0×10^8	1.9×10^6	89

$$\Gamma_e = \frac{1}{4}\left[\frac{17E_{\rm kin,iso}}{\pi n_{\rm ex} m_p c^5 t_{90}^3}\right]^{1/8} \approx 195\left(\frac{E_{\rm kin,iso}}{10^{54}\ {\rm ergs}}\right)^{1/8}\left(\frac{t_{90}}{10\ {\rm s}}\right)^{-3/8}\left(\frac{n_{\rm ex}}{1\ {\rm cm}^3}\right)^{-1/8}. \quad (9)$$

The reverse shock magnetic field in the comoving plasma frame is $B'_e = (8\pi\varepsilon_B n_{\rm ex} m_p c^2)^{1/2}$ and we set $\varepsilon_B = 0.1$ as in the internal shocks. The minimum Lorentz factor of the reverse shock-accelerated electrons in the un-shocked plasma frame is $\gamma'_{e,\rm min} \simeq \varepsilon_e(m_p/m_e)(\Gamma_i/\Gamma_e)$ and the peak electron synchrotron photon energy is $\epsilon'_{\gamma,\rm m} = \hbar c\Gamma_e(3\gamma'^2_{e,\rm min}eB'_e)/(2m_e c^2)$. However, the characteristic shock-accelerated electron Lorentz factor, from equating the synchrotron cooling time to the dynamic time: $t_{\rm dyn} = r_e/4\Gamma_e^2 c$, is $\gamma'_{e,c} = 6\pi m_e c/(\sigma_{\rm Th}B'^2_e\Gamma_e^4 t_{\rm dyn})$. The corresponding peak synchrotron photon energy radiated by these characteristic electrons in the same B'_e field is then

$$\epsilon'_{\gamma,c} = \hbar c\Gamma_e\frac{3\gamma'^2_{e,c}eB'_e}{2m_e c^2} \approx 0.4\left(\frac{E_{\rm kin,iso}}{10^{54}\ {\rm ergs}}\right)^{-25/24} \times \left(\frac{\Gamma_i}{300}\right)^{4/3}\left(\frac{t_{90}}{10\ {\rm s}}\right)^{9/8}\left(\frac{n_{\rm ex}}{1\ {\rm cm}^{-3}}\right)^{-11/24}{\rm eV}. \quad (10)$$

The number density of these photons in the reverse shock region is approximately given by the total synchrotron radiation power (typically at $\epsilon'_{\gamma,\rm m}$) by all electrons scaled at $\epsilon'_{\gamma,c}$ and then divided by $\epsilon'_{\gamma,c}$ as

$$n'_{\gamma,c} \simeq \frac{E_{\rm kin,iso}}{8\pi^2\hbar c r_e^2}\left(\frac{\Gamma_e}{\Gamma_i}\right)\frac{e^3B'_e}{m_e c^2 m_p c^2}\left(\frac{\epsilon'_{\gamma,\rm m}}{\epsilon'_{\gamma,c}}\right)^{1/2} \approx 6.8\times10^{12}\left(\frac{E_{\rm kin,iso}}{10^{54}\ {\rm ergs}}\right)^{11/12}\left(\frac{\Gamma_i}{300}\right)^{2/3} \times \left(\frac{t_{90}}{10\ {\rm s}}\right)^{-3/4}\left(\frac{n_{\rm ex}}{1\ {\rm cm}^{-3}}\right)^{19/12}{\rm cm}^{-3}. \quad (11)$$

The corresponding photon number spectrum is given by

$$\epsilon'_\gamma\frac{{\rm d}N'_\gamma}{{\rm d}\epsilon'_\gamma} \simeq n'_{\gamma,c}\times\begin{cases}(\epsilon'_\gamma/\epsilon'_{\gamma,c})^{-1/2}; & \epsilon'_{\gamma,\rm m} < \epsilon'_\gamma < \epsilon'_{\gamma,c},\\ (\epsilon'_\gamma/\epsilon'_{\gamma,c})^{-1}; & \epsilon'_\gamma > \epsilon'_{\gamma,c}.\end{cases} \quad (12)$$

Note that, one needs to explicitly calculate the proton to pion conversion efficiency factor f_π in the afterglow phase ($r_e > r_i$) as it may be lower than 0.2, contrary to the prompt (internal shocks) phase. We calculate f_π for reverse shock-accelerated protons to interact with photons of energy $\epsilon'_{\gamma,c}$ (Eq. (10)) at the Δ^+ resonance as

$$f_\pi = \min(1,\tau'_{p\gamma\to\Delta^+})\langle x_{p\to\Delta^+}\rangle \approx 0.2\left(\frac{E_{\rm kin,iso}}{10^{54}\ {\rm ergs}}\right)^{33/24}\left(\frac{t_{90}}{10\ {\rm s}}\right)^{-9/8}\left(\frac{n_{\rm ex}}{1\ {\rm cm}^{-3}}\right)^{9/8}, \quad (13)$$

where $\tau'_{p\gamma\to\Delta^+} \simeq \sigma_{p\gamma\to\Delta^+}(r_e/\Gamma_e)n'_{\gamma,c}$ is the optical depth using Eq. (11) and $\sigma_{p\gamma\to\Delta^+} = 5\times10^{-28}$ cm^2 is the pγ cross-section at the Δ^+ resonance. The neutrino break energy for the characteristic photon energy (Eq. (10)) is

Table 3
Afterglow neutrino flux parameters

GRB	f_π	$\mathscr{B}$ (GeV/cm^2/s)	$\epsilon_{\nu,b2}$ (GeV)	$\epsilon_{\nu,\rm max}$ (GeV)	$t_{\rm glow}$ (s)
050908	0.03	6.9×10^{-8}	1.5×10^{8}	1.4×10^{8}	20
050730	0.2	4.4×10^{-7}	2.5×10^{8}	2.8×10^{8}	155
050603	0.2	5.3×10^{-5}	1.0×10^{10}	6.0×10^{8}	10
020124A	0.2	2.1×10^{-6}	7.4×10^{8}	3.3×10^{8}	46
020813A	0.2	1.5×10^{-5}	2.0×10^{9}	8.4×10^{8}	89

$$\epsilon_{\nu,b2} = \frac{0.015\Gamma_e}{(1+z)}\left(\frac{\epsilon'_{\gamma,c}}{\rm GeV}\right)^{-1}{\rm GeV}. \quad (14)$$

The maximum shock-accelerated proton energy can be found by equating the shock-acceleration time to the shorter of the synchrotron cooling time (most efficient energy loss channel) and the dynamic time. The corresponding maximum neutrino energy is

$$\epsilon_{\nu,\rm max} = \frac{\langle x_{p\to\Delta^+}\rangle}{4(1+z)}(e\Gamma_e B'_e r_e) \quad (15)$$

in the afterglow phase. The resulting afterglow neutrino spectrum, following Eqs. (12)–(14), is

$$\epsilon_\nu^2\Phi^s_\nu = \frac{f_\pi}{8}\frac{S_\gamma}{t_{90}}\times\begin{cases}(\epsilon_\nu/\epsilon_{\nu,b2}); & \epsilon_\nu < \epsilon_{\nu,b2}\\ (\epsilon_\nu/\epsilon_{\nu,b2})^{1/2}; & \epsilon_{\nu,\rm max} \geqslant \epsilon_\nu \geqslant \epsilon_{\nu,b2}\end{cases} \quad (16)$$

for each neutrino flavor ν_μ, $\bar\nu_\mu$ and ν_e at the source. Again, the flavor ratios on Earth, after vacuum oscillation, would be $\Phi_{\nu_e+\bar\nu_e} = \Phi_{\nu_\mu+\bar\nu_\mu} = \Phi_{\nu_\tau+\bar\nu_\tau} = \Phi^s_\nu$, each with a duration of $t_{\rm glow} = t_{90}$. The parameters f_π, $\epsilon_{\nu,b2}$ and $\epsilon_{\nu,\rm max}$ are listed in Table 3 for each GRB. The pre-factor in the neutrino spectrum $\mathscr{B} = (f_\pi/8)(S_\gamma/t_{90})$, for different GRBs, is also listed in Table 3.

The formalism outlined above is schematically presented in Fig. 2, which qualitatively indicates the relationship between the neutrino and the photon spectra.

3.4. GRBs with incomplete data

We note ~100 GRBs (listed in Appendix) having insufficient electromagnetic data recorded while RICE was live. The break energy ($\epsilon_{\gamma,b}$) and spectral indices (α and β) of the γ-ray spectrum may be estimated (e.g., $\epsilon_{\gamma,b}$ from Eq. (3)) and/or sampled from their observed distributions. The relative error using the estimated spectral information is small and does not largely affect the neutrino flux predictions in the energy range where RICE is sensitive. However, the most important piece of information that is lacking is the redshift measurement. The luminosity and hence energy of a burst (see Eq. (1)) depends on the redshift or its luminosity distance. These in turn affect the model neutrino flux calculation. Various methods have been proposed to indirectly measure the redshift of a burst, e.g., from the time lag between the hard and soft γ-ray arrival from a burst [44,45]; using an empirical relation between the observed variability and the luminosity [46,47]; using observed

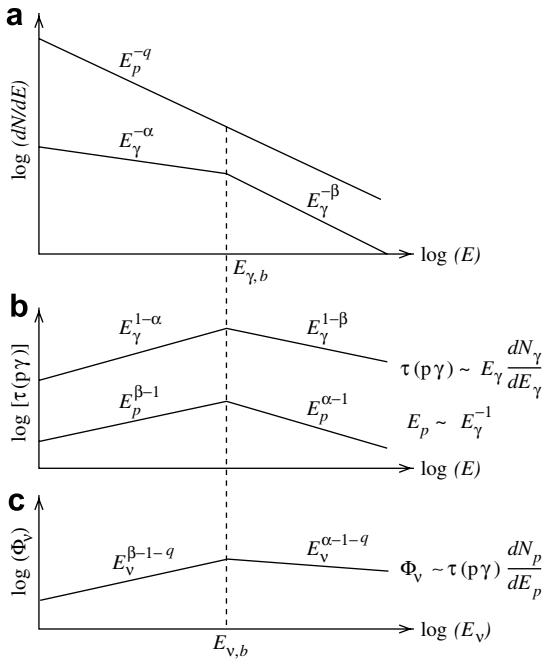

Fig. 2. Cartoon of the neutrino energy spectrum expected from a GRB having an observed γ-ray spectrum. (a) Shock accelerated proton spectrum: $\propto \epsilon_p^{-q}$, and broken power-law fit to the γ-ray spectrum: $\propto \epsilon_\gamma^{-\alpha}$ for $\epsilon_\gamma < \epsilon_{\gamma,b}$ and $\epsilon_\gamma > \epsilon_{\gamma,b}$. (b) Opacity for $p\gamma \to \Delta^+$ resonant interaction satisfying the condition $\epsilon_p\epsilon_\gamma = 0.3\Gamma^2$ GeV^2. Note that the optical depth changes its shape when expressed as a function of ϵ_p (lower curve) rather than ϵ_γ (upper curve) to satisfy the resonance condition $\epsilon_p\epsilon_\gamma = \text{const}$. (c) The neutrino spectrum follows the proton spectrum modulo the shape of the optical depth. At high energy (not shown here) above the synchrotron break energy (Eq. (5)), the neutrino spectrum would steepen by a factor of 2 in the spectral index.

correlation between γ-ray total and peak energy [48]; etc. For now, we have focused on those bursts for which reliable redshift data exist.

4. Search for gamma-ray burst coincidences

Software algorithms used to winnow the RICE data set are presented elsewhere [27–29]. Typically, antenna 'hits' must exceed a threshold corresponding to approximately $5.5\sigma_{\rm rms}$, where $\sigma_{\rm rms}$ is the rms noise in the recorded waveform for a given antenna channel. In cases for which the event time is known *a priori*, one can employ more sophisticated, albeit more time-consuming event reconstruction techniques. These include use of a 'matched filter' to search for lower-amplitude signals, thereby enhancing the effective volume. Although transients such as GRBs lend themselves to such approaches, we have not attempted such an analysis and instead rely on the results of previous RICE analyses for sensitivity and efficiency estimates.

We select gamma-ray bursts which were recorded within a ±1000 s overlap time window during which the RICE experiment was active [52]. Only GRBs which have declination angles less than zero and have therefore been localized to the southern hemisphere are considered, given the opacity of the earth to neutrinos at ultra-high energies. The recorded RICE experimental discriminator threshold allows a determination of the effective volume specifically for the run during which the gamma-ray burst was observed. The record of triggers, and software surface-noise vetoes over the 2000 s coincidence window allows an estimate of the average livetime fraction over that period. Relative to the published RICE effective volume and efficiency [29], our ultimate sensitivity is degraded by this calculated average livetime fraction.

Relative to the effective volume integrated over angle [29], appropriate for an expected isotropic (i.e., flat in both $dN/d(\cos\theta)$) and $dN/d\phi$) diffuse neutrino flux, we must determine the acceptance for point sources as a function of declination and azimuth. Our simulations indicate that the acceptance is constant (to within ∼10%) in azimuth

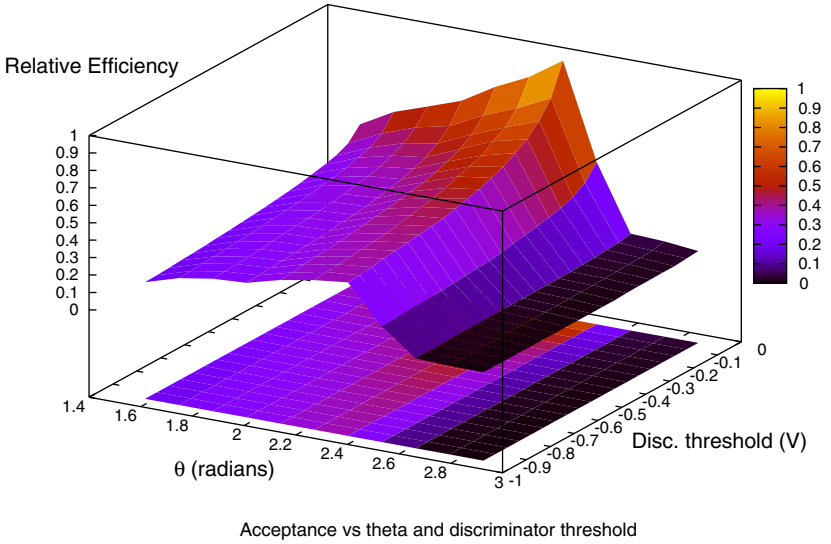

Fig. 3. Relative dependence of $V_{\rm eff}$ on nadir angle (i.e., π/2 + declination), and discriminator threshold, based on simulations of the RICE detector. π/2 corresponds to flux incident along the horizon; π corresponds to flux incident from zenith.

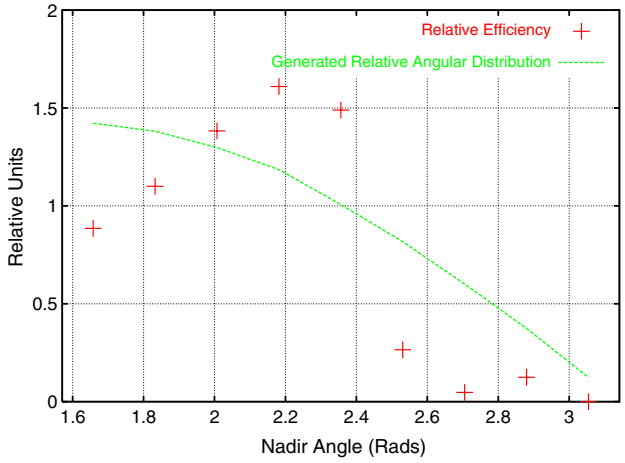

Fig. 4. Dependence of V_{eff} on nadir angle, integrated over energy. Also shown is the distribution of the expected incident flux. The overall efficiency is therefore the properly weighted average of the polar angle dependence.

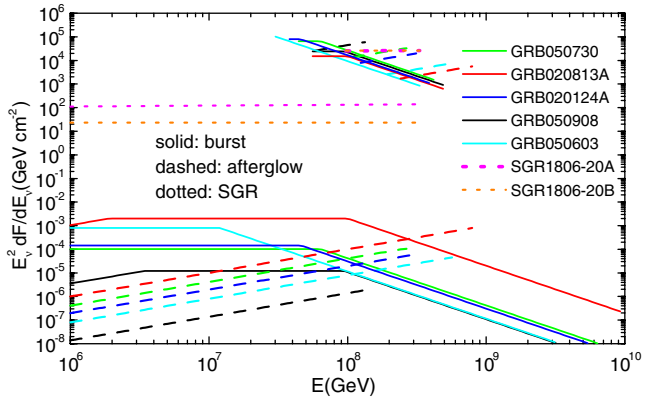

Fig. 5. Upper limit, derived from five indicated GRBs and for SGR 1806-20, assuming a 1:1:1 isoflavor mix at the detector. Lower set of lines indicate predicted GRB and SGR 1860-20 neutrino fluxes as described in the text; higher set of lines indicate RICE upper limits using previously published effective volumes and the expected angular dependence of the acceptance.

and that the dominant angular dependence is on the polar angle of the point source. Since the RICE array is shallow, the acceptance for neutrinos incident from the zenith (directly overhead) is nearly zero. Maximal acceptance is achieved for neutrinos incident closer to the horizon interacting in the 2.5 km of ice below the array which illuminate the array with a relative angle between the neutrino momentum vector and the vector to the array close to the Cherenkov angle. Fig. 3 shows the relative effective volume as a function of the discriminator threshold and the nadir angle of the incident neutrino. Given the fact that the angular dependence is more important than the energy dependence, Fig. 4 shows the angular dependence of the effective volume, integrated over energy. For each GRB, this graph provides a correction relative to the previously-published V_{eff} [29] using the tabulated declination angle for each analyzed GRB.

The non-observation of any in-ice shower candidates, coupled with the tabulated RICE neutrino-finding efficiency, allows an estimate of the expected event yield for GRB neutrino fluxes calculated as above. Our derived upper limits, following the prescription for relating a flux model to an upper limit as outlined in the previous RICE neutrino flux study [29], are presented in Fig. 5. We also list the limit values for each GRB in Table 4 and their ratios to the predicted flux values at a given neutrino energy. Simple linear scaling then may be used to get limit values at another energy.

An alternative approach to setting limits on the neutrino flux from individual GRBs is to use a source stacking method. These methods have been applied in gamma-ray astronomy and were discussed recently in the context of neutrinos from various classes of active galactic nuclei (AGNs) [49]. The total neutrino flux from all five GRBs in our sample, for the burst and afterglow models described, is displayed in Fig. 6. We derive upper limits on these total fluxes by following the same prescription as for the single burst analysis, using the sum of the number of events expected from each individual GRB.

A class of low luminosity, low energy (dominantly in the X-ray bands) bursts are known as X-ray flashes (XRFs). The typical break energy $\epsilon_{\gamma,\text{b}} \sim 1$–$10$ keV implies that protons need to be accelerated to $\gtrsim 10^{18}$ eV to produce neutrinos at these sources which is unlikely because of their low luminosity. Moreover, the proton to pion conversion efficiency f_π would be much lower in this case. There were three XRFs recorded while RICE was active namely GRBs 020903A, 030429A and 030723A (see Appendix) with bolometric fluences S_γ one to two orders of magnitude lower than typical long GRBs listed in Table 1.

Table 4
RICE limits and ratios to the predicted burst and afterglow fluxes at a given energy

GRB	Burst			Afterglow		
	ϵ_ν (GeV)	Limit (GeV/cm^2)	Ratio	ϵ_ν (GeV)	Limit (GeV/cm^2)	Ratio
050908	1.0×10^8	20152.48	2.01×10^9	1.0×10^8	44487.72	3.21×10^{10}
050730	1.0×10^8	24624.48	6.35×10^8	2.0×10^8	25037.32	3.04×10^8
050603	1.0×10^8	8613.60	8.13×10^8	2.0×10^8	2739.27	1.68×10^8
020124A	1.0×10^8	15436.97	5.44×10^8	2.0×10^8	12874.04	3.24×10^8
020813A	1.0×10^8	13975.23	7.55×10^6	3.0×10^8	2139.85	7.05×10^6

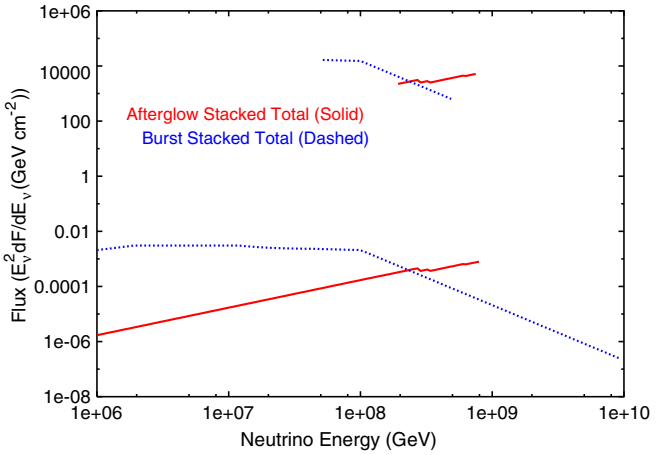

Fig. 6. Upper limit on the total stacked flux from the five GRBs, 020813, 020124, 050603, 050730 and 050908, assuming a 1:1:1 isoflavor mix at the detector. The lower pair of lines indicate the predicted total neutrino flux from the five GRBs for the burst and afterglow models for neutrino production; the higher set of lines indicate RICE upper limits for the total neutrino fluxes using previously published effective volumes and the expected angular dependence of the acceptance.

4.1. Other transient source searches

Soft gamma-ray repeaters (SGRs) represent one class of extreme X-ray pulsars repeatedly emitting ~0.1 s bursts of soft γ-rays. SGRs are highly magnetized (~10^{15} G) neutron stars, often called 'magnetars'. Four SGRs have been identified in the Milky Way (1806-20, 1627-41, 1900 + 14, and 1801-23) and one has been identified in the Large Magellanic Clouds (0526-66). Giant flares from an SGR, hypothesized to originate from a sudden shift of magnetic field, occur with periods of ~10 years. In particular, the giant flare of SGR 1806-20 on 27 December 2004 at 21:30:26 UT was the brightest cosmic transient observed to date with a flux ~10 ergs s^{-1} cm^{-2} lasting for ~0.1 s. We note that this flux is ~10^4 times larger than the most luminous GRBs ever detected. Detected radio afterglow of SGRs imply the presence of relativistic jets, similar to GRBs. If high energy neutrinos were emitted with comparable energy emitted in γ-rays, the 27 December 2004 giant flare of SGR 1806-20 might have been detected by operating neutrino telescopes, as predicted by several authors [50,51].

We investigated the possibility of a coincidence with the 27 December 04 SGR 1806-20 giant flare. Although the RICE experiment was active during that time, we did not observe a trigger at the time of the SGR flare. We did record two forced triggers ("unbiased" events) at 21:25:33 UT and 21:35:33 UT, respectively, which bracket the flare time by almost exactly five minutes. A channel-by-channel comparison of the time-domain and frequency-domain waveforms for these events reveals no obvious differences between the data recorded before-flare vs. after-flare. Given no detection we then put limits on two model fluxes

$$\epsilon_\nu^2 \Phi^s_{\nu,\mathrm{pp}} = 330 + 30 \ln\left(\frac{\epsilon_\nu}{\mathrm{GeV}}\right) \mathrm{GeV\ cm^{-2}\ s^{-1}} \quad \text{(Model A)},$$
$$\epsilon_\nu^2 \Phi^s_{\nu,\mathrm{p}\gamma} = 156\ \mathrm{GeV\ cm^{-2}\ s^{-1}} \quad \text{(Model B)}, \tag{17}$$

where Model A corresponds to the neutrino flux originating from pp interactions in Ref. [50] and Model B is a generic pγ flux, similar to the prediction in Ref. [51], assuming total proton energy is equal to the observed γ-ray energy. The maximum neutrino energy in both cases is 3.3×10^8 GeV [50]. The flux predictions and the limits are plotted in Fig. 5. The limits are 191 and 550 times higher than the flux predictions for Models A and B, respectively.

5. Summary

Selecting GRB events recorded while the RICE experiment was actively taking data, and using previously presented results on the RICE analysis procedures and simulations, we have estimated the expected RICE sensitivity to such transients. Based on the lack of observed coincidences, we set limits on the UHE neutrino flux for several candidates. Although the limits presented are well above model predictions, they do, nevertheless, probe possible neutrino fluxes from GRBs in an energy regime considerably higher than those previous studied. Future improvements in sensitivity will be realized by enlarging the scale of the radio detector array, as well as improved individual GRB parameter measurements.

Acknowledgments

This work was supported by the National Science Foundation Office of Polar Programs and the Department of Energy. We gratefully acknowledge the generous logistical support of the AMANDA and SPASE Collaborations (without whom this work would not have been possible), the National Science Foundation Office of Polar Programs under Grant No. 0338219, the University of Kansas, the University of Canterbury Marsden Foundation, and the Cottrell Research Corporation for their generous financial support. We also thank the winterovers who staffed the experiment during the last six years at the South Pole (Xinhua Bai, Allan Baker, Mike Boyce, Phil Broughton, Marc Hellwig, Matthias Leupold, Karl Mueller, Michael Offenbacher, Katherine Rawlins, Steffen Richter and Darryn Schneider), as well as the excellent on-site support offered by Raytheon Polar Services logistical personnel (particularly Rev. Al Baker, Jack Corbin, Joe Crane and Paul Sullivan). Any opinions, findings, and conclusions or recommendations expressed in this material are those of the author(s) and do not necessarily reflect the views of the National Science Foundation. SR was partially supported by NSF grant AST 0307376. We thank our RICE collaborators particularly Shahid Hussain, who supplied the computer code used to generate the flux upper limits presented here in, and Doug McKay, John Ralston, David

Seckel and Surujhdeo Seunarine for useful conversations and input. Alexey Provorov and Igor Zheleznykh (Moscow Institute of Nuclear Research, Moscow, Russia) constructed the TEM horn antennas currently used as part of the surface-noise veto. Derek Boyd performed important checks of the overall system timing calibration. John Paden and Matt Peters provided essential antenna expertise. George M. Frichter, Adrienne Juett, Tim Miller, Dave Schmitz, and Glenn Spiczak all performed essential work in the initial construction phases of this experiment.

Appendix. List of transients considered for matches

Included below are transients with full spectral information. Transient XRFs are insufficiently energetic for the current analysis.

SWIFT GRB/Time/Trigger/RA/Dec/Duration T90/Fluence (15–150 keV)/1-s Peak Photon Flux/Photon Index/XRT Initial Temporal Decay Index/XRT Spectral Index/(Gamma) Redshift/⟨*Livetime*⟩/D1 threshold
050908/05:42:31/154112/20.451 (01:21:48)/−12.962 (−1257:45)/20/4.91/0.70/1.86 (PL)/1.33/3.9/3.340/0.92/−0.389
050730/19:58:23/148225/212.063 (14:08:15.1)/−3.740 (−03:44:24.0)/155/24.2/0.57/1.52 (PL)/2.3/1.8/3.97/0.75/−0.370
050603/06:29:05/131560/39.982 (02:39:56)/−25.195 (−25:11:41)/13/76.3/27.6/1.17 (PL)/1.78/1.71/2.821/0.92/−0.385

HETE GRB/Time Class/Coords/Redshift/Epeak/T90/30–400 keV fluence (erg/cm^2)/lightcurve/⟨*Livetime*⟩/D1 threshold
GRB 020124A/10:41:15/XRR/09 h 32 m 49.0 s/−11d 27′ 34″/3.2/86.93/46.42/6.1e−06/0.83/−0.50
GRB 020813A/02:44:19/GRB/19h/46 m 37.9 s/−19d 35′ 16″/1.25/142.1/89.29/8.4e−05/0.98/−0.30
GRB 020903A/10:05:37/XRF/22 h 49 m 01.0 s/−20d 55′ 45″/0.25/5/4.10/1.6e−08/0.92/−0.22
GRB 030429A/10:42:22/XRF/12 h 13 m 06.0 s/−20d 55′ 59″/2.66/35.04/10.30/3.8e−07/0.95/−0.352
GRB 030723A/06:28:17/XRF/21 h 49 m 29.7 s/−27d 42′ 07″/2.3/11.3/6.78/2.8e−07/0.96/−0.352

GRBs recorded in southern hemisphere, with incomplete spectral or redshift information

GRB	Declination angle	⟨*Livetime*⟩	Discriminator threshold (V)
051111A	−2.64	0.79	−0.35
051109B	−53.959	0.946	−0.48
051021A	−45.519	0.916	−0.35
051013A	−4.399	0.886	−0.4
051007A	−0.512	0.868	−0.35
051006B	−67.715	0.958	−0.45
051004A	−10.869	0.94	−0.4

Appendix (*continued*)

GRB	Declination angle	⟨*Livetime*⟩	Discriminator threshold (V)
051004B	−15.347	0.946	−0.4
051001A	−30.4786	0.928	−0.47
050927A	−36.313	0.934	−0.44
050921A	−37.034	0.928	−0.43
050917A	−62.582	0.97	0.55
050917B	−21.242	0.934	−0.55
050916A	−50.5703	0.976	−0.57
050915B	−66.5899	0.958	−0.58
050915A	−27.9835	0.97	−0.58
050911A	−37.1506	0.85	−0.39
050910A	−29.775	0.928	−0.45
050908A	−11.0452	0.838	−0.39
050907A	−48.815	0.898	−0.39
050830B	−45.23	0.694	−0.36
050826A	−1.35683	0.856	−0.41
050822A	−45.9662	0.736	−0.41
050818A	−35.058	0.97	−0.51
050817A	−24.93	0.916	−0.44
050813A	−32.242	0.718	−0.4
050813B	−60.716	0.412	−0.4
050801A	−20.0719	0.886	−0.38
050728A	−26.984	0.766	−0.41
050727A	−21.768	0.922	−0.41
050726A	−31.9359	0.952	−0.41
052726B	−22.655	0.904	−0.41
050725A	−16.466	0.898	−0.42
050724A	−26.459	0.904	−0.40
050721A	−27.6189	0.454	−0.29
050721B	−1.44	0.826	−0.29
050715B	−0.059	0.514	−0.34
050714A	−15.528	0.754	−0.38
050713A	−12.264	0.604	−0.33
050709A	−37.0224	0.808	−0.31
050703A	−43.059	0.97	−0.51
050701A	−58.5844	0.478	−0.38
050701B	−1.4526	0.616	−0.47
050626A	−63.1342	0.388	−0.37
050623A	−27.331	0.838	−0.46
050614B	−42.492	0.874	−0.29
050612A	−63.6821	0.658	−0.38
050603A	−24.8182	0.88	−0.39
050602A	−20.198	0.874	−0.37
050509C	−43.1655	0.736	−0.45
050418A	−18.538	0.952	−0.40
050416A	−27.907	0.994	−0.23
050412A	−0.799	0.688	−0.42
050412B	−1.252	0.688	−0.42
050406A	−49.8125	0.934	−0.30
050402A	−20.422	0.802	−0.35
050331A	−40.5617	0.904	−0.29
050331B	−42.678	0.928	−0.29
050326A	−70.6288	0.934	−0.42

(*continued on next page*)

Appendix (*continued*)

GRB	Declination angle	⟨*Livetime*⟩	Discriminator threshold (V)
050326B	−71.375	0.922	−0.42
050323A	−40.582	0.844	−0.27
050323B	−20.417	0.916	−0.32
050322A	−42.093	0.832	−0.32
050318A	−45.6045	0.868	−0.24
050226A	−5.354	0.982	−0.55
050223A	−61.5275	0.904	−0.18
050222A	−53.777	0.856	−0.16
050219B	−56.2424	0.934	−0.28
050219A	−39.3172	0.904	−0.28
050217A	−43.036	0.964	−0.48
050213A	−53.791	0.91	−0.78
050211A	−20.41	0.856	−0.46
050203A	−52.384	0.43	−0.50
050202A	−38.72	0.266	−0.67
050130A	−20.405	0.85	−0.23
050129A	−43.013	0.598	−0.21
050121A	−20.387	0.01	−0.59
050121B	−37.84	0.976	−0.59
050108A	−37.848	0.04	−0.18
050107A	−20.409	0.97	−0.56
050107B	−15.637	0.892	−0.56
041224A	−5.344	0.97	−0.88
041223A	−36.9271	0.322	−0.78
040730A	−55.5492	0.922	−0.17
040330A	−20.4104	0.91	−0.33
040309A	−20.3924	0.832	−0.30
040228A	−16.612	0.892	−0.37
040223A	−40.0667	0.244	−0.34
031015A	−20.525	0.976	−0.65
030821A	−44.6431	0.988	−0.87
030725A	−49.3178	0.982	−0.35
030723A	−26.2868	0.92	−0.28
030716A	−67.8673	0.934	−0.28
030706A	−47.4994	0.976	−0.35
030629A	−42.571	0.976	−0.28
030528A	−21.3806	0.964	−0.29
030429A	−19.0862	0.94	−0.35
030418A	−6.972	0.976	−0.35
030323A	−20.2297	0.592	−0.62
021021A	−0.38333	0.868	−0.35
020903A	−19.0708	0.892	−0.22
020813A	−18.3987	0.976	−0.30
020812A	−4.70056	0.952	−0.24
020801A	−52.2297	0.952	−0.35
020629B	−17.2772	0.976	−0.35
020305A	−13.6967	0.982	−0.50
020124A	−10.5406	0.52	−0.50

References

[1] G.J. Fishman, C.A. Meegan, Annu. Rev. Astron. Astrophys. 33 (1995) 415.
[2] J. van Paradijs, C. Kouveliotou, R.A.M.J. Wijers, Annu. Rev. Astron. Astrophys. 38 (2000) 379.
[3] M. Vietri, Astrophys. J 453 (1995) 883.
[4] E. Waxman, Phys. Rev. Lett. 75 (1995) 386.
[5] K. Greisen, Phys. Rev. Lett. 16 (1966) 748.
[6] F.W. Stecker, Astrophys. J. 228 (1979) 919.
[7] R. Engel, D. Seckel, T. Stanev, Phys. Rev. D 64 (2001) 093010.
[8] E. Waxman, J. Bahcall, Phys. Rev. Lett. 78 (1997) 2292.
[9] E. Waxman, J. Bahcall, Phys. Rev. D 59 (1999) 023002.
[10] E. Waxman, J.N. Bahcall, Astrophys. J 541 (2000) 707.
[11] F. Halzen, D. Hooper, Rept. Prog. Phys. 65 (2002) 1025.
[12] D. Guetta, D. Hooper, J. Alvarez-Muñiz, F. Halzen, E. Reuveni, Astropart. Phys. 20 (2004) 429.
[13] S. Razzaque, P. Mészáros, E. Waxman, Phys. Rev. D 69 (2004) 023001.
[14] J. Alvarez-Muñiz, F. Halzen, D. Hooper, Astrophys. J. 604 (2004) L85.
[15] M. Stamatikos, J. Kurtzweil, M.J. Clarke. Available from: <arXiv: astro-ph/0510336>.
[16] J.K. Becker, M. Stamatikos, F. Halzen, W. Rhode, Astropart. Phys. 25 (2006) 118.
[17] E. Zas, F. Halzen, T. Stanev, Phys. Lett. B257 (1991) 432; E. Zas, F. Halzen, T. Stanev, Phys. Rev. D45 (1992) 362.
[18] J. Alvarez-Muñiz et al., Phys. Rev. D68 (2003) 043001; J. Alvarez-Muñiz et al., Phys. Rev. D62 (2000) 063001; J. Alvarez-Muñiz et al. Available from: <arXiv:astro-ph/0512337>.
[19] S. Razzaque et al., Phys. Rev. D65 (2002) 103002.
[20] S. Razzaque et al., Phys. Rev. D69 (2004) 047101.
[21] R.V. Buniy, J.P. Ralston, Phys. Rev. D65 (2002) 016003.
[22] S. Hussain, D. McKay, Phys. Rev. D70 (2004) 103003.
[23] J. Alvarez-Muñiz, R.A. Vázquez, E. Zas, Phys. Rev. D61 (2000) 023001.
[24] S. Mandal, S. Klein, J.D. Jackson, Phys. Rev. D72 (2005) 093003.
[25] S. Barwick et al., J. Glac. 51 (2005) 231–238.
[26] P.B. Price, 1995. Available from: <astro-ph/951011>; P.B. Price, Astropart. Phys. 5 (1996) 43.
[27] I. Kravchenko et al., Astropart. Phys. 19 (2003) 15–36.
[28] I. Kravchenko et al. (The RICE Collaboration); I. Kravchenko et al., Astropart. Phys. 20 (2003) 195.
[29] I. Kravchenko et al., Phys. Rev. D 73 (2006) 082002.
[30] P. Mészáros, Annu. Rev. Astron. Astrophys. 40 (2002) 137.
[31] T. Piran, Phys. Rep. 314 (1999) 575.
[32] P. Mészáros, E. Waxman, Phys. Rev. Lett. 87 (2001) 171102.
[33] S. Razzaque, P. Mészáros, E. Waxman, Phys. Rev. D 68 (2003) 083001.
[34] C.D. Dermer, A. Atoyan, Phys. Rev. Lett. 91 (2003) 071102.
[35] Z.G. Dai, T. Lu, Astrophys. J. 551 (1999) 249.
[36] J. Granot, D. Guetta, Phys. Rev. Lett. 90 (2003) 191102.
[37] D. Guetta, J. Granot, Phys. Rev. Lett. 90 (2003) 201103.
[38] S. Razzaque, P. Mészáros, E. Waxman, Phys. Rev. Lett. 90 (2003) 241103.
[39] E. Waxman, Lect. Notes Phys. 576 (2001) 122. Available from: astro-ph/0103186.
[40] S. Razzaque, P. Mészáros in: S. Sarkar, D. Hooper (Eds.), The IceCube Yellow Book, in preparation.
[41] http://nedwww.ipac.caltech.edu/.
[42] D. Band et al., Astrophys. J. 413 (1993) 281.
[43] G. Ghirlanda, G. Ghisellini, C. Firmani, Mon. Not. R. Astron. Soc. 361 (2005) L10.
[44] J.P. Norris, Astrophys. J. 579 (2002) 386.
[45] J.T. Bonnel et al., Astrophys. J. 490 (1997) 79.
[46] D.E. Reichart et al., Astrophys. J. 552 (2001) 57.
[47] E.F. Fenimore, E. Ramirez-Ruiz. Available from: <astro-ph/0004176>.
[48] L. Amati et al., A&A 390 (2002) 81.
[49] A. Achterberg et al., The IceCube collaboration, Astropart. Phys., in press.

[50] K. Ioka, S. Razzaque, S. Kobayashi, P. Mészáros, Astrophys. J. 633 (2005) 1013.
[51] F. Halzen, H. Landsman, T. Montaruli. Available from: <arXiv:astro-ph/0503348>.
[52] "hits-*" files were scanned from http://kuhep4.phsx.ku.edu/~iceman/data/, using the data format descriptions given in http://kuhep4.phsx.ku.edu/~iceman/rice2002.ps, The RICE Monte Carlo simulation is publicly accessible from http://kuhep4.phsx.ku.edu/~iceman/ricemc05.bz2.
[53] We follow the original Waxman–Bahcall estimate, which took the ratio of $\pi^+:\pi^0 = 1:1$. The true ratio (from isospin) is 1:2.